Research Article

Enabling D2D Transmission Mode of Reconfigurable Intelligent Surfaces Aided in Wireless NOMA System

Viet-Dung Le[1] ⓘ*, Hong-Nhu Nguyen*[2,*] ⓘ*, Sang Quang Nguyen*[3] ⓘ*, Trong-Tu Bui*[1] ⓘ*, Dinh Cong Hien*[4]*, Byung Seo Kim*[5] ⓘ

[1]Faculty of Electronics and Telecommunication, University of Science, 227 Nguyen Van Cu Street, District 5, Ho Chi Minh City, Vietnam
[2]Faculty of Electronics and Telecommunications, Saigon University, 273 An Duong Vuong Street, District 5, Ho Chi Minh City, Vietnam
[3]Posts and Telecommunications Institute of Technology Ho Chi Minh City, Vietnam
[4]Major Projects/Field Operations/Commissioning Department, North Oil Company, Qatar
[5]Department of Software and Communications Engineering, Hongik University, Sejong, South Korea

levdung@hcmus.edu.vn, nhu.nh@sgu.edu.vn, sangnq@ptit.edu.vn, tubt@hcmus.edu.vn, conghien201085@gmail.com, jsnbs@hongik.ac.kr

*Corresponding author: Hong-Nhu Nguyen; nhu.nh@sgu.edu.vn

Abstract. *Reconfigurable Intelligent Surfaces (RISs) are emerging as a promising alternative for future wireless networks. This study investigates device-to-device (D2D) communication systems using non-orthogonal multiple access (NOMA) and RISs between user devices and base stations to enhance the performance of the proposed system. The closed-form and approximate-form expressions of outage probability (OP) were demonstrated with the impact of imperfect successful interference cancelation (ipSIC) to give more key insight into our work. Finally, the Monte Carlo simulation is adopted to clarify the accuracy of the analysis of mathematical expressions.*

Keywords

imperfect SIC (ipSIC), non-orthogonal multiple access (NOMA), outage probability (OP), reconfigurable intelligent surface (RIS).

1.　Introduction

Reconfigurable Intelligent Surfaces (RISs) is a programmable surface structure that can control electromagnetic wave reflection. RISs can steer signals to the receiver resulting in better reception or link quality. Furthermore, the wireless channel usually distorts transmitted signals in wireless communications. RIS enables the manipulation of surfaces within radio channels to steer signals in targeted directions, thereby enhancing the reliability and energy efficiency of wireless systems. By precisely controlling how waves interact with their environment, RIS can focus signals toward specific areas, reducing interference and optimizing power usage, which ultimately leads to more stable and energy-conscious network performance. The fading channel always impacts the transmission of the signal in wireless networks, the study explores IRS-assisted NOMA networks for both downlink and uplink scenarios, where an IRS is strategically deployed to enhance network coverage. Specifically, the IRS aids a user device located at the edge of the cell, enabling more reliable communication with the base station, which is particularly beneficial in areas where signal strength is typically weak [1]. Energy issues are an im-

portant consideration in wireless relay networks. Numerous attempts have aimed to improve the efficiency of energy use at the relay nodes. The authors in [2–6] have explored the simultaneous use of radio frequency (RF) signals for both energy harvesting and data transmission. This dual-purpose approach is emerging as an innovative solution for promoting green energy in wireless communication systems. In [7, 8], the self-energy recycling (S-ER) protocol has been introduced for full-duplex multi-relay networks, where it involves capturing and storing energy derived from self-interference at the relay stations. This method leverages the energy from interference generated during simultaneous transmission and reception to enhance the overall energy efficiency of the network. Besides, to improve the transmission efficiency of wireless networks. In which security is considered as a cooperative transmission protocol for system application. Physical layer security has been considered and proposed the system models by the authors [9–13]. In the context of IoT networks, the auhors in [14] has explored the security and reliability of power splitting-based relaying with the aid of a jammer, highlighting the performance superiority of dynamic PS relaying (DPSR) over static PS relaying (SPSR) in terms of outage and intercept probabilities under various system parameters. The authors in [15] provide a detailed performance analysis of a time-switching energy harvesting strategy for half-duplex bidirectional wireless sensor networks over Rician fading channels, offering exact expressions for outage probability, throughput, and symbol-error-rate under hardware impairments. Recent work explores energy harvesting-based two-way half-duplex relaying sensor networks, deriving exact and upper bound ergodic capacity and symbol error ratio over Rayleigh fading channels, with validation through Monte Carlo simulations [16, 17]. The authors in [18] investigated the performance of a device-to-device (D2D) communication network, where a source node transmits data using harvested energy from a power beacon to overcome energy constraints, while both the destination and an eavesdropper are subject to co-channel interference from other sources using the same frequency. .

In cooperative communication, two primary relaying strategies are commonly employed: Decode-and-Forward (DF) and Amplify-and-Forward (AF). In the DF approach, the relay node decodes the received signal before re-encoding and forwarding it to the destination, which can mitigate noise but may introduce decoding errors [19–22]. On the other hand, AF relays simply amplify the received signal, preserving the signal's original noise characteristics, which leads to a more straightforward implementation but may result in noise amplification [23]. Both techniques offer significant improvements in communication reliability and capacity, particularly in environments with fading and interference.

The evolution of mobile communications continues at a rapid pace, with emerging demands and complexities associated with the 6th generation (6G) and future advancements. As technology progresses, the field is faced with new and intricate requirements that must be addressed to meet the expectations of next-generation communication systems. Reconfigurable intelligent surfaces (RIS) can help extend wireless coverage, RIS empowers network operators to manage the scattering, reflection, and refraction properties of radio waves. This capability allows for the mitigation of adverse effects commonly associated with natural wireless propagation, thereby enhancing overall network performance and reliability [24, 25]. The study explores IRS-assisted networks, evaluating the effects of both imperfect successive interference cancellation (ipSIC) and perfect successive interference cancellation (pSIC) techniques. This investigation, detailed in the referenced work, examines how these two approaches impact network performance under varying conditions [26].

Non-orthogonal multiple access (NOMA) networks and power transfer schemes combine to support the users used. In [27], NOMA (Non-Orthogonal Multiple Access) and full-duplex techniques are leveraged to significantly enhance spectral efficiency. By integrating these two approaches, the system maximizes data transmission capabilities and optimizes the use of available frequency resources. The study explores the use of Device-to-Device (D2D) communications for relaying transmissions to improve communication reliability. As detailed in [28, 29], the authors demonstrated a scenario where D2D communication is facilitated by an Energy Harvesting (EH) assisted relay. In this setup, signals are transmitted from a Base Station (BS) to both conventional cellular users and D2D users, leveraging EH technology to enhance the overall system performance. The study examines the application of non-orthogonal multiple access (NOMA) in traditional relaying networks, highlighting its role in managing large-scale connections. Integrating NOMA with Reconfigurable Intelligent Surfaces (RIS) is proposed as a groundbreaking approach to achieving energy-efficient and intelligent wireless communication. RIS, characterized by its two-dimensional structure and numerous passive elements, enhances network performance by optimizing signal propagation and energy efficiency [30, 31]. To assess the realistic end-to-end performance of the system in question, the studies in [32–34] modeled both transmission hops such as experiencing independent, though not necessarily identically distributed, extended Generalized-K fading. Our new analytical approach presents a formula derived using the bivariate H-Fox function, which provides a refined evaluation

of the system's performance under different fading conditions. An efficient algorithm H-Fox function is also proposed to evaluate the average bit error probability. Besides, the simultaneously transmitting and reflecting reconfigurable intelligent surface (STAR-RIS) is emerging as a promising technology for the sixth generation (6G) wireless communication landscape. STAR-RIS enhances the ability to achieve extremely low power transmission while providing seamless coverage by enabling surfaces to both transmit and reflect signals concurrently. This dual capability positions STAR-RIS as a key enabler for future wireless networks, addressing the need for efficient energy use and uninterrupted service coverage [35–38].

Different above discussions, our main contributions can be listed as followings:

- We analyze the outage performance (OP) of NOMA systems assisted by RIS in D2D networks.

- The OP's analytical expressions are derived for a network with two NOMA users positioned on opposite sides of the STAR-RIS.

- Determine and evaluate whether increasing the number of RIS elements enhances the system's performance. Finally, the correctness of mathematical frameworks are conducted by Monte Carlo simulation.

There are various portions to the paper. Section 2 outlines the system and channel model employed in the study. The mathematical expressions for the Outage Probability (OP) of two users is examined in section 3. Section 4 contains the system's closed-form OP approximations. Section 5 describe the Monte Carlo method to validate all derivations. Finally, Section 6 provides the conclusion of the paper.

2. System and Channel Model

2.1. System Model

As shown in Fig. 1, we introduce the system model for a RIS-aided relaying system that utilizes decode and forward (DF) technique, where the first hop is a radio frequency (RF)-RIS and the second hop is a RIS-RF transmissions, respectively. We assumed that the base station (BS) and nearby user (D_1) are unlikely to communicate directly because of obstacles, the BS connects to the D_1 via a RIS (RIS-1) located on a structure. Communication between near user D_1 and the far user (D_2) is also established via another RIS (RIS-2). RIS acts as an intermediary medium between BS and D_1 to ensure a direct line of sight path between the two nodes. It is assumed that all nodes possess perfect
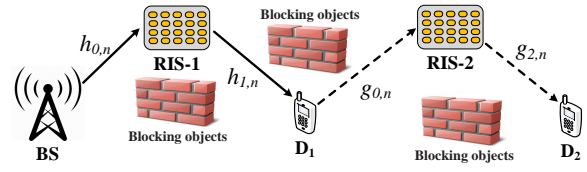

Fig. 1: Illustration of RIS-aided NOMA network model.

channel state information (CSI) and are equipped with a single antenna [1]. We have N_1 and N_2 reflecting elements in RIS-1 and RIS-2, respectively. For simplicity, we assume that the two RIS devices are identical, i.e. $N = N_1 = N_2$. The Rayleigh fading distribution is pursued by surface RF networks employing BS-RIS-1-D_1 and D_1-RIS-2-D_2 connections.

During the first time slot, BS will transmit the superimposed signal to D_1 with the help of a RIS-1, where x_i and a_i are the signal and power allocation coefficients of user i, respectively. It should be noticed that $a_1 + a_2 = 1$. Following the NOMA principle, we assume that $a_2 > a_1$ if D_2's QoS needs are greater than D_1. As a result, the baseband signal received at D_1 reflected by RIS-1 is provided by

$$\bar{y}_{D_1} = \left(\sum_{n=1}^{N_1} h_{0,n} h_{1,n} \varepsilon_n^h\right)\left(\sqrt{a_1 P_{BS}} x_1 + \sqrt{a_2 P_{BS}} x_2\right) + \bar{\omega}_{D_1},$$

$$(1)$$

where P_{BS} denotes the transmit power of BS, $\varepsilon_n^h = \varpi_n^h\left(\phi_n^h\right)e^{j\phi_n^h}$ is the RIS-1 reflection coefficient produced by the nth reflector; $\varpi_n^h\left(\phi_n^h\right) = 1$ is the ideal phase shifts $(n = 1, 2, \ldots, N)$; x_1 and x_2 denote the D_1 and D_2 transmitted signals, respectively; $\bar{\omega}_{D_1}$ denotes the additive white Gaussian noise (AWGN) at the BS with variance N_0 and $\phi_n^h \in [0, 2\pi)$ is the RIS-1 phase-shift variable of the nth element $\forall n \in N_1$. Moreover, we have $h_{0,n} = \bar{h}_{0,n} e^{j\vartheta_n^h}\big/\sqrt{d_{h_0}^\alpha}$ and $h_{1,n} = \bar{h}_{1,n} e^{j\theta_n^h}\big/\sqrt{d_{h_1}^\alpha}$ in which ϑ_n^h and θ_n^h are the channel phases, d_{h_0} and d_{h_1} denote the distances from the BS to RIS-1 and RIS-1 to D_1, respectively, α is the path-loss exponent. Following [24], we assume that RIS-1 accurately well-knows the values ϑ_n^h and θ_n^h.

D_1 first decodes x_2 by treating the signal from x_1 as interference, and the corresponding signal-to-interference-plus noise ratio (SINR) is written as follows:

$$\bar{\gamma}_{D_1, x_2} = \frac{a_2 P_{BS} d_{h_0}^{-\alpha} d_{h_1}^{-\alpha}\left|\sum_{n=1}^{N_1} e^{j\left(\phi_n^h - \vartheta_n^h - \theta_n^h\right)}\bar{h}_{1,n}\bar{h}_{0,n}\right|^2}{a_1 P_{BS} d_{h_0}^{-\alpha} d_{h_1}^{-\alpha}\left|\sum_{n=1}^{N_1} e^{j\left(\phi_n^h - \vartheta_n^h - \theta_n^h\right)}\bar{h}_{1,n}\bar{h}_{0,n}\right|^2 + N_0}.$$

$$(2)$$

As indicated in [25], the reflected signals must be co-phased by $\phi_n^h = \vartheta_n^h + \theta_n^h$. Therefore, the maximum

SINR at D_1 to detect x_2 can be expressed as a

$$\bar{\gamma}_{D_1,x_2} = \frac{a_2 P_{BS} d_{h_0}^{-\alpha} d_{h_1}^{-\alpha} |A|^2}{a_1 P_{BS} d_{h_0}^{-\alpha} d_{h_1}^{-\alpha} |A|^2 + N_0}$$
$$= \frac{a_2 \rho d_{h_0}^{-\alpha} d_{h_1}^{-\alpha} |A|^2}{a_1 \rho d_{h_0}^{-\alpha} d_{h_1}^{-\alpha} |A|^2 + 1}, \quad (3)$$

where $\rho = \frac{P_{BS}}{N_0}$ is the transmit signal-to-noise radio (SNR) of BS, $A \triangleq \sum_{n=1}^{N_1} |\bar{h}_{0,n}| |\bar{h}_{1,n}|$ with $\bar{h}_{0,n} \sim \mathcal{CN}(0, \lambda_{h_0})$ and $\bar{h}_{1,n} \sim \mathcal{CN}(0, \lambda_{h_1})$.

After implementing SIC, x_1 signal is detected with the SNR is given by

$$\bar{\gamma}_{D_1,x_1}^{\text{ipSIC}} = \frac{a_1 \rho d_{h_0}^{-\alpha} d_{h_1}^{-\alpha} |A|^2}{\varpi \rho |h_I|^2 + 1}, \quad (4a)$$

$$\bar{\gamma}_{D_1,x_1}^{\text{pSIC}} = a_1 \rho d_{h_0}^{-\alpha} d_{h_1}^{-\alpha} |A|^2, \quad (4b)$$

where $\varpi \in [0,1]$. Specifically, $\varpi = 0$ and $\varpi = 1$ represent perfect successive interference cancellation (pSIC) and imperfect successive interference cancellation (ipSIC), respectively. It is assumed that the residual interference from ipSIC follows Rayleigh fading, with the complex channel coefficient denoted as $h_I \sim \mathcal{CN}(0, \lambda_I)$, as described in [26].

In the second time slot, the D_1 sent a message $\sqrt{P_{D_1}} x_2$ to D_2 by virtue of a RIS-2. Hence, the signals received at D_2 is

$$\bar{y}_{D_2} = \left(\sum_{n=1}^{N_2} g_{0,n} g_{2,n} \varepsilon_n^g \right) \sqrt{P_{D_1}} x_2 + \bar{\omega}_{D_2}, \quad (5)$$

where P_{D_1} is the power at D_1, $\bar{\omega}_{D_2}$ denote the AWGN at D_2 with equal variance N_0, $g_{0,n} = \bar{g}_{0,n} e^{j\vartheta_n^g} / \sqrt{d_{g_0}^\alpha}$ and $g_{2,n} = \bar{g}_{2,n} e^{j\theta_n^g} / \sqrt{d_{g_2}^\alpha}$ d_{g_0} and d_{g_2} denote the distances from the D_1 to RIS-2 and RIS-2 to D_2, respectively, and $\varepsilon_n^g = \varpi_n^g (\phi_n^g) e^{j\phi_n^g}$ is defined similarly to (1).

Similarly, we assume the phase shifts of the RIS-2 elements are selected to maximize the received signal energy. It can be shown SNR detects signal x_2 at NOMA user D_2 as

$$\bar{\gamma}_{D_2} = \rho d_{g_0}^{-\alpha} d_{g_2}^{-\alpha} |B|^2, \quad (6)$$

where $B \triangleq \sum_{n=1}^{N_2} |\bar{g}_{0,n}| |\bar{g}_{2,n}|$ with $\bar{g}_{0,n} \sim \mathcal{CN}(0, \lambda_{g_0})$ and $\bar{g}_{2,n} \sim \mathcal{CN}(0, \lambda_{g_2})$. By asuming $P_{D_1} = P_{BS}$ then $\rho = \frac{P_{D_1}}{N_0}$.

2.2. Channel Model

Before computing outage probability, the probability distribution function (PDF) of channel $|h_I|^2$ is given by [27]

$$f_{|h_I|^2}(x) = \frac{1}{\lambda_I} e^{-\frac{x}{\lambda_I}}. \quad (7)$$

In terms of the corresponding cumulative distribution function (CDF) of channel $|h_I|^2$, $F_{|h_I|^2}(x)$ is given as

$$F_{|h_I|^2}(x) = 1 - e^{-\frac{x}{\lambda_I}}. \quad (8)$$

Based on [30], the PDF and CDF of the cascade channel gain of $|A|^2$ and $|B|^2$ can be given as, respectively.

$$f_{|A|^2}(x) = \frac{2x^{\frac{N-1}{2}}}{\Gamma(N) \left(\sqrt{\lambda_{h_0}\lambda_{h_1}}\right)^{N+1}} K_{N-1} \left(2\sqrt{\frac{x}{\lambda_{h_0}\lambda_{h_1}}}\right),$$
$$(9a)$$

$$f_{|B|^2}(x) = \frac{2x^{\frac{N-1}{2}}}{\Gamma(N) \left(\sqrt{\lambda_{g_0}\lambda_{g_2}}\right)^{N+1}} K_{N-1} \left(2\sqrt{\frac{x}{\lambda_{g_0}\lambda_{g_2}}}\right),$$
$$(9b)$$

and

$$F_{|A|^2}(x) = 1 - \frac{2x^{\frac{N}{2}}}{\Gamma(N) \left(\sqrt{\lambda_{h_0}\lambda_{h_1}}\right)^N} K_N \left(2\sqrt{\frac{x}{\lambda_{h_0}\lambda_{h_1}}}\right),$$
$$(10a)$$

$$F_{|B|^2}(x) = 1 - \frac{2x^{\frac{N}{2}}}{\Gamma(N) \left(\sqrt{\lambda_{g_0}\lambda_{g_2}}\right)^N} K_N \left(2\sqrt{\frac{x}{\lambda_{g_0}\lambda_{g_2}}}\right),$$
$$(10b)$$

where $K_v(.)$ is so-called the Bessel function and $\Gamma(.)$ is the Gamma function.

3. Outage Probability

3.1. Outage Probability of D_2

The outage probability of D_2 in the downlink phase can be expressed by

$$P_{D_2} = \text{Pr}\left(\min\left(\frac{\bar{\gamma}_{D_1,x_2}}{\gamma_{th2}}, \frac{\bar{\gamma}_{D_2}}{\gamma_{th2}}\right) < 1\right)$$
$$= 1 - \text{Pr}\left(\bar{\gamma}_{D_1,x_2} > \gamma_{th2}, \bar{\gamma}_{D_2} > \gamma_{th2}\right), \quad (11)$$

where $\gamma_{thi} = 2^{2R_i} - 1$, $i \in \{1,2\}$ with R_i being the target rate at D_i.

Entering (3) and (6) into (11), P_{D_2} is computed by

$$P_{D_2} = 1 - \text{Pr}\left(|A|^2 > \varphi_2\right) \text{Pr}\left(|B|^2 > \varphi_1\right)$$
$$= 1 - \left[1 - F_{|A|^2}(\varphi_2)\right] \left[1 - F_{|B|^2}(\varphi_1)\right]$$
$$= F_{|B|^2}(\varphi_1) + F_{|A|^2}(\varphi_2) - F_{|A|^2}(\varphi_2) F_{|B|^2}(\varphi_1), \quad (12)$$

where $\varphi_1 = \frac{\gamma_{th2}}{\rho d_{g_0}^{-\alpha} d_{g_2}^{-\alpha}}$ and $\varphi_2 = \frac{\gamma_{th2}}{\rho d_{h_0}^{-\alpha} d_{h_1}^{-\alpha}(a_2 - \gamma_{th2} a_1)}$.

Plugging (10a) and (10b) into (12), we have the outage probability of D_2 is calculated as

$$
\begin{aligned}
P_{D_2} =& 1 - \frac{4(\varphi_1\varphi_2)^{\frac{N}{2}}}{\Gamma(N)^2 \left(\sqrt{\lambda_{h_0}\lambda_{h_1}\lambda_{g_0}\lambda_{g_2}}\right)^N} \\
& \times K_N\left(2\sqrt{\frac{\varphi_2}{\lambda_{h_0}\lambda_{h_1}}}\right) K_N\left(2\sqrt{\frac{\varphi_1}{\lambda_{g_0}\lambda_{g_2}}}\right).
\end{aligned}
\tag{13}
$$

Note (13) is derived on the condition of $a_2 > \gamma_{th2}a_1$.

3.2. Outage Probability of D_1

In the case of pSIC when $\varpi = 0$, the outage probability of D_1 with pSIC can be calculated as

$$
\begin{aligned}
P_{D_1}^{pSIC} =& \Pr\left(\min\left(\frac{\bar{\gamma}_{D_1,x_2}}{\gamma_{th2}}, \frac{\bar{\gamma}_{D_1,x_1}^{pSIC}}{\gamma_{th1}}\right) < 1\right) \\
=& 1 - \Pr\left(\bar{\gamma}_{D_1,x_2} > \gamma_{th2}, \bar{\gamma}_{D_1,x_1}^{pSIC} > \gamma_{th1}\right) \\
=& 1 - \Pr\left(|A|^2 > \varphi_2, |A|^2 > \varphi_3\right) \\
=& 1 - \Pr\left(|A|^2 > \varphi_{\max}\right) = F_{|A|^2}(\varphi_{\max}),
\end{aligned}
\tag{14}
$$

where $\varphi_3 = \frac{\gamma_{th1}}{a_1\rho d_{h_0}^{-\alpha} d_{h_1}^{-\alpha}}$ and $\varphi_{\max} = \max(\varphi_2, \varphi_3)$.

Substituting (10a) into (14), $P_{D_1}^{pSIC}$ is written as

$$
P_{D_1}^{pSIC} = \frac{2\varphi_{\max}^{\frac{N}{2}}}{\Gamma(N)\left(\sqrt{\lambda_{h_0}\lambda_{h_1}}\right)^N} K_N\left(2\sqrt{\frac{\varphi_{\max}}{\lambda_{h_0}\lambda_{h_1}}}\right).
\tag{15}
$$

Scenario of ipSIC when $\varpi = 1$, the outage probability of D_1 with ipSIC can be calculated as

$$
\begin{aligned}
P_{D_1}^{ipSIC} =& \Pr\left(\min\left(\frac{\bar{\gamma}_{D_1,x_2}}{\gamma_{th2}}, \frac{\bar{\gamma}_{D_1,x_1}^{ipSIC}}{\gamma_{th1}}\right) < 1\right) \\
=& 1 - \Pr\left(\bar{\gamma}_{D_1,x_2} > \gamma_{th2}, \bar{\gamma}_{D_1,x_1}^{ipSIC} > \gamma_{th1}\right).
\end{aligned}
\tag{16}
$$

Theorem 1. *The closed-form expression for the outage probability of D_1 is given by (15) next top page, in which $G_{p,q}^{m,n}[.]$ is the Meijer G-function and $\mathcal{H}_{p,q:u,v:e,f}^{n,m:s,t:i,j}(.)$ is the extended generalized bivariate Fox's H-function (EGBFHF)* * *as defined in [33, Eq. (2.57)]*

---

*Both a MATLAB and MATHEMATICA implementation of the EGBFHF are provided in [32] and [34] .

Proof: From (16), $P_{D_1}^{ipSIC}$ is calculated as

$$
\begin{aligned}
P_{D_1}^{ipSIC} =& 1 - \Pr\left(|A|^2 > \varphi_2, |A|^2 > \varphi_3\left(\rho|h_I|^2 + 1\right)\right) \\
=& 1 - \Pr\left(|A|^2 > \varphi_2, |h_I|^2 < \frac{|A|^2}{\rho\varphi_3} - \frac{1}{\rho}, |A|^2 > \varphi_3\right) \\
=& 1 - \Pr\left(|A|^2 > \varphi_{\max}, |h_I|^2 < \frac{|A|^2}{\rho\varphi_3} - \frac{1}{\rho}\right),
\end{aligned}
\tag{18}
$$

Based on (9a) and (7), (17) can be calculated as

$$
\begin{aligned}
P_{D_1}^{ipSIC} =& 1 - \int_{\varphi_{\max}}^{\infty} f_{|A|^2}(x) \int_0^{\frac{x}{\rho\varphi_3} - \frac{1}{\rho}} f_{|h_I|^2}(y) dx dy \\
=& 1 - \frac{2}{\Gamma(N)\left(\sqrt{\lambda_{h_0}\lambda_{h_1}}\right)^{N+1}}[I_1 - I_2],
\end{aligned}
\tag{19}
$$

where $I_1 = \int_{\varphi_{\max}}^{\infty} x^{\frac{N-1}{2}} K_{N-1}\left(2\sqrt{\frac{x}{\lambda_{h_0}\lambda_{h_1}}}\right) dx$ and $I_2 = \int_{\varphi_{\max}}^{\infty} x^{\frac{N-1}{2}} K_{N-1}\left(2\sqrt{\frac{x}{\lambda_{h_0}\lambda_{h_1}}}\right) e^{-\frac{x}{\lambda_I\rho\varphi_3} + \frac{1}{\lambda_I\rho}} dx$.

To solve the integrals I_1, we utilize the following transformations involving the Meijer G-function [39, Chap.8.4]

$$
H(1 - |x|) = G_{1,1}^{1,0}\left(x \left|\begin{array}{c} 1 \\ 0 \end{array}\right.\right),
\tag{20}
$$

$$
H(|x| - 1) = G_{1,1}^{0,1}\left(x \left|\begin{array}{c} 1 \\ 0 \end{array}\right.\right),
\tag{21}
$$

$$
e^{-ax} = G_{0,1}^{1,0}\left(ax \left|\begin{array}{c} - \\ 0 \end{array}\right.\right),
\tag{22}
$$

$$
K_v(x) = \frac{1}{2} G_{0,2}^{2,0}\left(\frac{x^2}{4} \left|\begin{array}{c} -, - \\ \frac{v}{2}, \frac{-v}{2} \end{array}\right.\right),
\tag{23}
$$

where $H(x)$ is unit step function as
$$
H(x) = \begin{cases} 1, x > 0 \\ 0, x < 0 \end{cases}
$$

We have I_1 is rewritten as follows

$$
\begin{aligned}
I_1 =& \int_{\varphi_{\max}}^{\infty} x^{\frac{N-1}{2}} K_{N-1}\left(2\sqrt{\frac{x}{\lambda_{h_0}\lambda_{h_1}}}\right) dx \\
=& \int_0^{\infty} H\left(\frac{x}{\varphi_{\max}} - 1\right) x^{\frac{N-1}{2}} K_{N-1}\left(2\sqrt{\frac{x}{\lambda_{h_0}\lambda_{h_1}}}\right) dx \\
=& \frac{1}{2} \int_0^{\infty} G_{1,1}^{0,1}\left(\frac{x}{\varphi_{\max}} \left|\begin{array}{c} 1 \\ 0 \end{array}\right.\right) x^{\frac{N-1}{2}} \\
& \times G_{0,2}^{2,0}\left(\frac{x}{\lambda_{h_0}\lambda_{h_1}} \left|\begin{array}{c} - \\ \frac{N-1}{2}, \frac{1-N}{2} \end{array}\right.\right) dx.
\end{aligned}
\tag{24}
$$

$$
\begin{aligned}
P_{D_1}^{ipSIC} =& 1 - \frac{2}{\Gamma(N)\left(\sqrt{\lambda_{h_0}\lambda_{h_1}}\right)^{N+1}} \left[\frac{\varphi_{\max}(\lambda_{h_0}\lambda_{h_1})^{\frac{N-1}{2}}}{2} G_{1,3}^{3,0}\left(\frac{\varphi_{\max}}{\lambda_{h_0}\lambda_{h_1}} \ \middle| \ \begin{matrix} 0 \\ -1, N-1, 0 \end{matrix} \right) \right. \\
& \left. - \frac{(\lambda_{h_0}\lambda_{h_1})^{\frac{N+1}{2}} e^{\frac{1}{\lambda_I \rho}}}{2} \mathcal{H}_{2,0:0,1:1,1}^{0,2:1,0:0,1}\left(\begin{matrix} (1-N;1,1),(0;1,1) \\ - \end{matrix} \ \middle| \ \begin{matrix} - \\ (0,1) \end{matrix} \ \middle| \ \begin{matrix} (1,1) \\ (0,1) \end{matrix} \ \middle| \ \frac{\lambda_{h_0}\lambda_{h_1}}{\lambda_I \rho \varphi_3}, \frac{\lambda_{h_0}\lambda_{h_1}}{\varphi_{\max}} \right) \right].
\end{aligned}
\tag{17}
$$

Let $t = \frac{x}{\lambda_{h_0}\lambda_{h_1}} \Rightarrow \lambda_{h_0}\lambda_{h_1}t = x \Rightarrow \lambda_{h_0}\lambda_{h_1}dt = dx$; then, I_1 can be rewritten as

$$
\begin{aligned}
I_1 =& \frac{(\lambda_{h_0}\lambda_{h_1})^{\frac{N+1}{2}}}{2} \int_0^\infty G_{1,1}^{0,1}\left(\frac{\lambda_{h_0}\lambda_{h_1}t}{\varphi_{\max}} \ \middle| \ \begin{matrix} 1 \\ 0 \end{matrix} \right) t^{\frac{N-1}{2}} \\
& \times G_{0,2}^{2,0}\left(t \ \middle| \ \begin{matrix} - \\ \frac{N-1}{2}, \frac{1-N}{2} \end{matrix} \right) dt.
\end{aligned}
\tag{25}
$$

Based on [40, Eq. (9.31.5), Eq. (7.811.1)] and applying some polynomial expansion manipulations

$$
\begin{aligned}
I_1 =& \frac{(\lambda_{h_0}\lambda_{h_1})^{\frac{N+1}{2}}}{2} \int_0^\infty G_{1,1}^{0,1}\left(\frac{\lambda_{h_0}\lambda_{h_1}t}{\varphi_{\max}} \ \middle| \ \begin{matrix} 1 \\ 0 \end{matrix} \right) \\
& \times G_{0,2}^{2,0}\left(t \ \middle| \ \begin{matrix} - \\ N-1, 0 \end{matrix} \right) dt \\
=& \frac{\varphi_{\max}(\lambda_{h_0}\lambda_{h_1})^{\frac{N-1}{2}}}{2} G_{1,3}^{3,0}\left(\frac{\varphi_{\max}}{\lambda_{h_0}\lambda_{h_1}} \ \middle| \ \begin{matrix} 0 \\ -1, N-1, 0 \end{matrix} \right).
\end{aligned}
\tag{26}
$$

Finally, with the help of (23), (22), (21), I_2 is calculated as

$$
\begin{aligned}
I_2 =& \int_{\varphi_{\max}}^\infty x^{\frac{N-1}{2}} K_{N-1}\left(2\sqrt{\frac{x}{\lambda_{h_0}\lambda_{h_1}}} \right) e^{-\frac{x}{\lambda_I \rho \varphi_3} + \frac{1}{\lambda_I \rho}} dx \\
=& e^{\frac{1}{\lambda_I \rho}} \int_0^\infty x^{\frac{N-1}{2}} e^{-\frac{x}{\lambda_I \rho \varphi_3}} H\left(\frac{x}{\varphi_{\max}} - 1 \right) \\
& \times K_{N-1}\left(2\sqrt{\frac{x}{\lambda_{h_0}\lambda_{h_1}}} \right) dx \\
=& \frac{e^{\frac{1}{\lambda_I \rho}}}{2} \int_0^\infty x^{\frac{N-1}{2}} G_{0,1}^{1,0}\left(\frac{x}{\lambda_I \rho \varphi_3} \ \middle| \ \begin{matrix} - \\ 0 \end{matrix} \right) G_{1,1}^{0,1}\left(\frac{x}{\varphi_{\max}} \ \middle| \ \begin{matrix} 1 \\ 0 \end{matrix} \right) \\
& \times G_{0,2}^{2,0}\left(\frac{x}{\lambda_{h_0}\lambda_{h_1}} \ \middle| \ \begin{matrix} - \\ \frac{N-1}{2}, \frac{1-N}{2} \end{matrix} \right) dx.
\end{aligned}
\tag{27}
$$

After referring to the identities [41, Eq. (2.3)], I_2 can be formulated as (28)

Substituting (28) and (26) into (18), we can obtain (17). The proof is completed.

3.3. Optimal Outage Performance Analysis

Based on the calculated outage probability expressions, it is difficult to establish closed-form equations for the best values of power allocation factors a_1, a_2. Fortunately, we may use low-complexity algorithms based on the golden section search approach to solve this problem. For example, in Algorithm 1, we demonstrate how to get the exact value of a_2 that minimizes the first user's OP. Algorithm 1's accuracy is mostly dependent on the step search Δ.

Algorithm 1 Optimization Algorithm to find a_2^* based on Golden section search

---
LeftleftThisthisUpup UnionUnionFindCompressFindCompress InputInputOutputOutput Initialize $\psi_{\min} = 0$, $\psi_{\max} = 1$, the golden section search $\varpi = \frac{\sqrt{5}-1}{2}$ and a stopping threshold $\Delta = 10^{-3}$ The optimal of a_2^* that minimum the outage performance $P_1^\star(a_2^*)$, $\star \in \{ipSIC, pSIC\}$
Create sets $\beta_1 = \psi_{\max} - (\psi_{\max} - \psi_{\min})\varpi$ and $\beta_2 = \psi_{\min} + (\psi_{\max} - \psi_{\min})\varpi$
$|\psi_{\max} - \psi_{\min}| \leq \Delta$ Update: $P_{\text{temp1}}^\star = P_1^\star(\beta_1)$
Update: $P_{\text{temp2}}^\star = P_1^\star(\beta_2)$
$P_1^\star(\bullet)$ is given by (17) and (15) $P_{\text{temp1}}^\star < P_{\text{temp2}}^\star$ Update: $\psi_{\max} \leftarrow \beta_2$ Update: $\psi_{\min} \leftarrow \beta_1$ Update: $\beta_1 \leftarrow \psi_{\max} - (\psi_{\max} - \psi_{\min})\varpi$
Update: $\beta_2 \leftarrow \psi_{\min} + (\psi_{\max} - \psi_{\min})\varpi$
The optimal of $a_2^* = (\psi_{\max} + \psi_{\min})/2$

Although optimal OP may be found in some circumstances, the analytical findings of OP performance remain complex, making acquiring any insights challenging. This prompts us to investigate the approximate calculation of the primary system performance measures in the next section.

4. The Approximation of Outage Probability

Theorem 2. *The asymptotic outage probability of D_2 at high SNRs for the situations $N = 1$ and $N \geq 2$ is*

$$
\begin{aligned}
I_2 &= \frac{e^{\frac{1}{\lambda_I \rho}}}{2} \int_0^\infty x^{\frac{N+1}{2}-1} G_{0,2}^{2,0}\left(\frac{x}{\lambda_{h_0}\lambda_{h_1}} \middle| \begin{array}{c} - \\ \frac{N-1}{2}, \frac{1-N}{2} \end{array}\right) G_{0,1}^{1,0}\left(\frac{x}{\lambda_I \rho \varphi_3} \middle| \begin{array}{c} - \\ 0 \end{array}\right) G_{1,1}^{0,1}\left(\frac{x}{\varphi_{\max}} \middle| \begin{array}{c} 1 \\ 0 \end{array}\right) dx \\
&= \frac{(\lambda_{h_0}\lambda_{h_1})^{\frac{N+1}{2}} e^{\frac{1}{\lambda_I \rho}}}{2} \mathcal{H}_{2,0:0,1:1,1}^{0,2:1,0:0,1}\left(\begin{array}{c} (1-N;1,1),(0;1,1) \\ - \end{array} \middle| \begin{array}{c} - \\ (0,1) \end{array} \middle| \begin{array}{c} (1,1) \\ (0,1) \end{array} \middle| \frac{\lambda_{h_0}\lambda_{h_1}}{\lambda_I \rho \varphi_3}, \frac{\lambda_{h_0}\lambda_{h_1}}{\varphi_{\max}}\right).
\end{aligned}
\tag{28}
$$

given by the following equations:

$$
P_{D_2}^\infty = \begin{cases} 1 - \prod_{l=1}^2 \left[\frac{2\varphi_l}{\xi_i}\ln\left(\sqrt{\frac{\varphi_l}{\xi_i}}\right)+1\right] & , N=1 \\ \sum_{l=1}^2 \frac{\varphi_l}{\xi_l(N-1)} - \prod_{l=1}^2 \frac{\varphi_l}{\xi_i(N-1)} & , N \geq 2 \end{cases}
\tag{29}
$$

where $\xi_1 = \lambda_{h_0}\lambda_{h_1}$ and $\xi_2 = \lambda_{g_0}\lambda_{g_2}$.

Proof: To make the computation easier, we use the series form of the Bessel function $K_n(x)$ to approximate the high SNR. We have $K_n(x)$ can be approximated when $n=1$ and $n \geq 2$ as

$$
K_1(x) \approx \frac{x}{2}\ln\left(\frac{x}{2}\right) + \frac{1}{x},
\tag{30}
$$

$$
K_n(x) \approx \left[\frac{2^n(n-1)!}{x^n} - \frac{2^{n-2}(n-2)!}{x^{n-2}}\right]\frac{1}{2}.
\tag{31}
$$

Equation (29) can be obtained by putting (31) and (30) into (13), respectively. The proof is finished.

Similarly, by solving $P_{D_2}^\infty$, the asymptotic expression for D_1 with pSIC is calculated by

$$
P_{D_1}^{pSIC,\infty} = \begin{cases} -\frac{2\varphi_{\max}}{\lambda_{h_0}\lambda_{h_1}}\ln\left(\sqrt{\frac{\varphi_{\max}}{\lambda_{h_0}\lambda_{h_1}}}\right) & , N=1 \\ \frac{\varphi_{\max}}{\lambda_{h_0}\lambda_{h_1}(N-1)} & , N \geq 2 \end{cases}
\tag{32}
$$

Finally, when $\rho \to \infty$ then results can be obtained easily by using two approximate equations, namely, $\bar{\gamma}_{D_1,x_2}^\infty \approx \frac{a_2}{a_1}$ and $\bar{\gamma}_{D_1,x_1}^{\mathrm{ipSIC},\infty} \approx \frac{a_1 d_{h_0}^{-\alpha} d_{h_1}^{-\alpha} A^2}{|h_I|^2}$. Thereby at high SNRs, we can write the approximate expression for the D_1 with ipSIC as follows:

$$
P_{D_1}^{ipSIC,\infty} = \begin{cases} 1 - \Pr\left(\bar{\gamma}_{D_1,x_1}^{\mathrm{ipSIC},\infty} > \gamma_{th1}\right) & , a_2 > a_1\varphi_2 \\ 1 & \text{otherwise.} \end{cases}
\tag{33}
$$

Substituting (10a) and (7) into (33), $P_{D_1}^{ipSIC,\infty}$ is written as

$$
\begin{aligned}
P_{D_1}^{ipSIC,\infty} &= 1 - \Pr\left(A^2 > \chi|h_I|^2\right) \\
&= 1 - \int_0^\infty f_{|h_I|^2}(x)\left[1 - F_{|A|^2}(\chi x)\right]dx \\
&= 1 - \frac{2\chi^{\frac{N}{2}}}{\lambda_I \Gamma(N)\left(\sqrt{\lambda_{h_0}\lambda_{h_1}}\right)^N} \\
&\quad \times \int_0^\infty x^{\frac{N}{2}} e^{-\frac{x}{\lambda_I}} K_N\left(2\sqrt{\frac{\chi x}{\lambda_{h_0}\lambda_{h_1}}}\right)dx,
\end{aligned}
\tag{34}
$$

where $\chi = \frac{\gamma_{th1}}{a_1 d_{h_0}^{-\alpha} d_{h_1}^{-\alpha}}$. Now, we set $t^2 = x \to 2tdt = dx$ and using [?, Eq. (6.631.3)], $P_{D_1}^{ipSIC,\infty}$ can be calculated by

$$
\begin{aligned}
P_{D_1}^{ipSIC,\infty} &= 1 - N\left(\sqrt{\frac{\lambda_I \chi}{\lambda_{h_0}\lambda_{h_1}}}\right)^{N-1} e^{\left(\frac{\lambda_I \chi}{2\lambda_{h_0}\lambda_{h_1}}\right)} \\
&\quad \times W_{\frac{-N-1}{2},\frac{N}{2}}\left(\frac{\lambda_I \chi}{\lambda_{h_0}\lambda_{h_1}}\right),
\end{aligned}
\tag{35}
$$

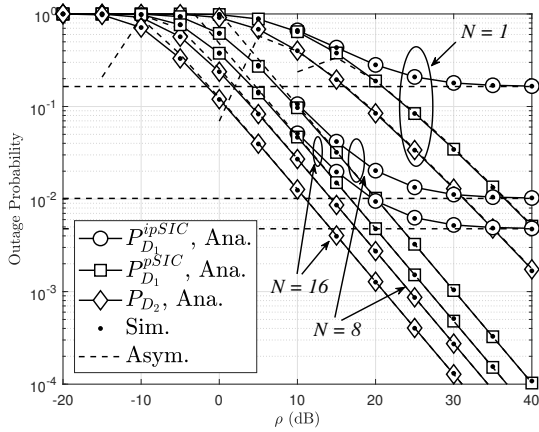where $W_{\lambda,\mu}(x)$ is so-called Whittaker function.

5.   Results and Discussion

In this section, we utilize Monte Carlo simulations [42–45] (designated as 'Sim.') to corroborate the precise analyses (designated as 'Ana.') and asymptotic results (designated as 'Asym.'). The target rate has unit of bit per channel user and is denoted in short as BPCU. These simulations are performed in accordance with the parameters delineated in Table 1. It is noteworthy that our computational framework integrates technological advancements by employing symbolic computations within computer by running code, thereby facilitating the attainment of exact outcomes.

Fig. 2 show the OP of D_1 and D_2, respectively, versus the transmit SNR, ρ (dB), with different RIS elements. The simulated outcomes align with the respective analytical findings for the RIS-supported NOMA network. For $N=2$, the outage probability remains relatively elevated throughout the SNR spectrum. For $N=8$ and $N=16$, the outage probability exhibits
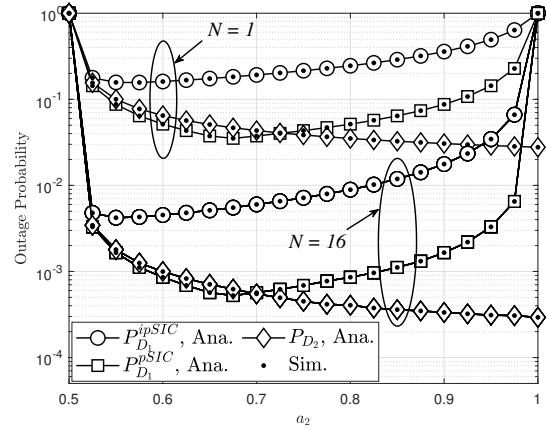
Tab. 1: Definition of system parameters [31, 35, 36]

Notation	Values	Notation	Values
a_1	0.1	d_{g_2}	60 m
a_2	0.9	α	2
R_1	1 BPCU	λ_{h_0}	0.4
R_2	1 BPCU	λ_{h_1}	0.6
d_{h_0}	40 m	λ_{g_0}	0.4
d_{h_1}	60 m	λ_{g_2}	0.6
d_{g_0}	40 m	λ_{h_I}	0.01

Fig. 2: Outage probability versus ρ at D_1 and D_2.

Fig. 3: Outage probabilities versus a_2, with $R_1 = R_2 = 0.5$, $\lambda_I = 0.1$ and $\rho = 20$ [dB].
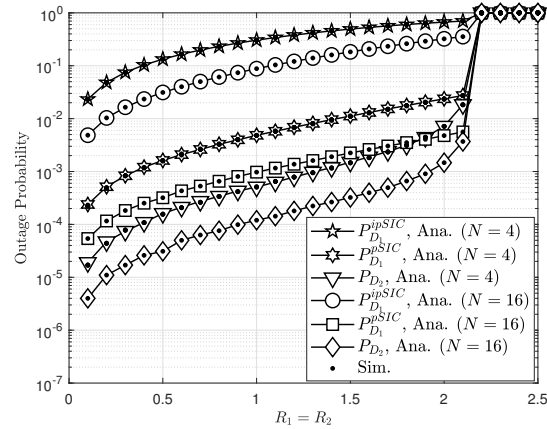
Fig. 4: Outage performance versus fixed data rates R_1 and R_2, with $a_1 = 0.05$, $a_2 = 0.95$, $\lambda_I = 0.1$ and $\rho = 30$ [dB].

a significant reduction as the quantity of reflecting elements increases. An augmented number of reflecting elements within the RIS enhances the capability to manipulate the wireless environment, resulting in improved signal strength and diminished outage occurrences. This underscores the advantages of incorporating a greater number of reflecting elements to improve wireless communication efficacy. The pSIC method demonstrates a lower outage probability than the ipSIC, indicating superior performance under less-than-ideal conditions. The analytical outcomes correspond closely with simulation findings, particularly at elevated SNR levels, thereby affirming the precision of the theoretical frameworks. In conclusion, the quantity of RIS reflecting elements is pivotal in minimizing outage probability, with increased values of N resulting in enhanced performance across the spectrum.

Fig 3 illustrates the relationship between the outage probability and the power allocation factor a_2 for different numbers of reflecting elements N in RIS. The graph compares analytical results for different SIC methods and also includes simulation data, with a focus on identifying the optimal power allocation factor. The optimal power allocation factor a_2 (around 0.7) minimizes outage probability for both users and RIS configurations, regardless of the number of reflecting elements. Increasing the number of reflecting elements N from

4 to 16 significantly reduces the outage probability, demonstrating the importance of RIS in improving system performance. The optimal power allocation strikes a balance between the two users, highlighting the importance of resource management in multi-user RIS-assisted systems.

Fig. 4 illustrates the correlation between the outage probability and the target rates $R_1 = R_2$, for two users operating within a system that employs a RIS. This analysis juxtaposes various quantities of reflecting elements N present in the RIS and assesses the system's performance under both perfect and imperfect SIC conditions. An increase in the target rate $R_1 = R_2$ corresponds with a rise in the outage probability, particularly for elevated rates (exceeding 1.5 BPCU), where the system encounters difficulties in sustaining performance. Systems characterized by a greater number of reflecting elements ($N = 16$) demonstrate significantly superior performance relative to those with a lesser count of elements ($N = 4$), indicating that the RIS can substantially bolster system reliability through

effective modulation of the wireless environment. pSIC results in lower outage probabilities than ipSIC, especially at high target rates, emphasizing the importance of efficient interference cancellation. In conclusion, the figure elucidates the influence of both the target rate and the quantity of reflecting elements on the outage probability within a RIS-assisted framework. An increased number of reflecting elements alongside perfect SIC culminates in enhanced performance, particularly at higher target rates.

6. Conclusion

In this study, we have proposed a model D2D for RIS-NOMA aided in the environment with blocking objects. First, we derived closed-form expressions for the outage probabilities at D_1, D_2, and the increased number of RIS. In order to enhance the efficacy of the system, a low-complexity 2D golden section search is executed, taking into account the power allocation parameters for NOMA with the aim of reducing the outage probabilities for devices experiencing imperfect SIC as well as those benefiting from perfect SIC. Simulation results show that the effectiveness of perfect SIC is better than imperfect SIC with an increase in RISs. The use of multiple devices and RIS to improve the performance of the NOMA system with dynamically moving users such as cars and nonlinear energy harvesting is left for future work.

Acknowledgment

Author Contributions

Viet-Dung Le, Dinh Cong Hien, and Sang Quang Nguyen developed the system model. Hong-Nhu Nguyen and Trong-Tu Bui performed the analytical calculations and numerical simulations, while B-S KIM wrote the whole paper. All authors contributed to the final version of the manuscript.

References

[1] CHENG, Y., LI, K. H., LIU, Y., TEH, K. C. and POOR, H. V. Downlink and uplink intelligent reflecting surface aided networks: NOMA and OMA. *IEEE Transactions on Wireless Communications*, vol. 20, no. 6, pp. 3988-4000, 2021. DOI: 10.1109/TWC.2021.3054841.

[2] NGUYEN, S. Q., and HYUNG YUN KONG. Generalized Diversity Combining of Energy Harvesting Multiple Antenna Relay Networks: Outage and Throughput Performance Analysis. *Annals of Telecommunications*, vol. 71, no. 5, pp. 265–277, 2016. DOI: 10.1007/s12243-016-0508-9.

[3] V-D. PHAN, T.N. NGUYEN, A.V. LE, and M. VOZNAK. A Study of Physical Layer Security in SWIPT-Based Decode-and-Forward Relay Networks with Dynamic Power Splitting. *Sensors*, vol. 21, no. 17, art.no.5692, 2021. DOI: 10.3390/s21175692.

[4] TIN, P. T., NGUYEN, T. N., TRAN, D. H., VOZNAK, M., PHAN, V. D., and CHATZINOTAS, S. Performance enhancement for full-duplex relaying with time-switching-based SWIPT in wireless sensors networks. *Sensors*, vol. 21, no. 11, art.no. 3847, 2021. DOI: 10.3390/s21113847.

[5] NGUYEN, T. N., TRAN, M., NGUYEN, T. L., HA, D. H., and VOZNAK, M. Performance analysis of a user selection protocol in cooperative networks with power splitting protocol-based energy harvesting over Nakagami-m/Rayleigh channels. *Electronics*, vol. 8, no. 4, art.no. 448, 2019. DOI: 10.3390/electronics8040448.

[6] C.T. DUNG, et.al. Secrecy performance of multi-user multi-hop cluster-based network with joint relay and jammer selection under imperfect channel state information. *Performance Evaluation*, vol. 147, art.no. 102193, 2021. DOI: 10.1016/j.peva.2021.102193.

[7] T. N. NGUYEN, T. T. DUY, P. T. TRAN, M. VOZNAK, X. LI, and H. V. POOR. Partial. Full Relay Selection Algorithms for AF Multi-Relay Full-Duplex Networks With Self-Energy Recycling in Non-Identically Distributed Fading Channels. *IEEE Transactions on Vehicular Technology*, vol. 71, no. 6, pp. 6173-6188, 2022, DOI: 10.1109/TVT.2022.3158340.

[8] T. N. NGUYEN, T. VAN CHIEN, V. Q. DINH, L. -T. TU, M. VOZNAK, and Z. DING. Outage Probability Analysis for Relay-Aided Self-Energy Recycling Wireless Sensor Networks Over INID Rayleigh Fading Channels. *IEEE Sensors Journal*, vol. 24, no. 7, pp. 11184-11194, 1 April, 2024, DOI: 10.1109/JSEN.2024.3365698.

[9] TRAN TIN, P., THE HUNG, D., NUYEN, T. N., DUY, T. T., and VOZNAK, M. Secrecy performance enhancement for underlay cognitive radio

networks employing cooperative multi-hop transmission with and without presence of hardware impairments. *Entropy*, vol. 21, no. 2, art.no. 217, 2021. DOI: 10.3390/e21020217.

[10] D. -H. HA, T. N. NGUYEN, M. H. Q. TRAN, X. LI, P. T. TRAN, and M. VOZNAK. Security and Reliability Analysis of a Two-Way Half-Duplex Wireless Relaying Network Using Partial Relay Selection and Hybrid TPSR Energy Harvesting at Relay Nodes. *IEEE Access*, vol. 8, pp. 187165-187181, 2020. DOI: 10.1109/ACCESS.2020.3030794.

[11] T. N. NGUYEN, et al. Security–Reliability Trade-off Analysis for SWIPT- and AF-Based IoT Networks With Friendly Jammers. *IEEE Internet of Things Journal*, vol. 9, no. 21, pp. 21662-21675, 2022. DOI: 10.1109/JIOT.2022.3182755.

[12] MINH, B. V., NGUYEN, T. N., and TU, L. T. Physical layer security in wireless sensors networks: secrecy outage probability analysis. *Journal of Information and Telecommunication*, pp. 1-23, 2024. DOI: 10.1080/24751839.2024.2352961.

[13] SANG, N. Q., and KONG, H. Y. Improving Secrecy Outage and Throughput Performance in Two-Way Energy-Constraint Relaying Networks Under Physical Layer Security. *Wireless Personal Communications* , vol. 96, pp. 6425–6457, 2017. DOI: 10.1007/s11277-017-4485-8.

[14] T. MINH, et al. Security and Reliability Analysis of the Power Splitting-Based Relaying in Wireless Sensors Network. *Sensors*, vol. 24, no. 4, 2024. DOI: 10.3390/s24041300.

[15] N. N. TAN, et al. Energy Harvesting over Rician Fading Channel: A Performance Analysis for Half-Duplex Bidirectional Sensor Networks under Hardware Impairments. *Sensors*, vol. 18, no. 6, 2018. DOI: 10.3390/s18061781.

[16] P. T. TIN, et al. Exploiting Direct Link in Two-Way Half-Duplex Sensor Network over Block Rayleigh Fading Channel: Upper Bound Ergodic Capacity and Exact SER Analysis. *Sensors*, vol. 20, no. 4, 2020. DOI: 10.3390/s20041165.

[17] T. M. HOANG, et al. Performance and optimal analysis of time-switching energy harvesting protocol for MIMO full-duplex decode-and-forward wireless relay networks with various transmitter and receiver diversity techniques. *Journal of the Franklin Institute*, vol. 357, no. 17, pp. 13205-13230, 2020. DOI: 10.1016/j.jfranklin.2020.09.037.

[18] B. V. MINH, et al. D2D Communication Network with the Assistance of Power Beacon under the Impact of Co-channel Interferences and Eavesdropper: Performance Analysis. *Advances in Electrical and Electronic Engineering*, vol. 21, no. 4, 2023. DOI: 10.15598/aeee.v21i4.5495.

[19] N. N. Tan, et al. Performance enhancement for energy harvesting based two-way relay protocols in wireless ad-hoc networks with partial and full relay selection methods. *Ad Hoc Networks*, vol. 84, 2019. DOI: 10.1016/j.adhoc.2018.10.005.

[20] N. N. Tan, et al. Two-Way Half Duplex Decode and Forward Relaying Network with Hardware Impairment over Rician Fading Channel: System Performance Analysis. *ELEKTRONIKA IR ELEKTROTECHNIKA*, vol. 24, no. 2, 2018. DOI: 10.5755/j01.eie.24.2.20639.

[21] N. N. TAN, et al. Adaptive relaying protocol for decode and forward full-duplex system over Rician fading channel: System performance analysis. *China Communications*, vol. 16, no. 3, 2019. DOI: 10.12676/j.cc.2019.03.009.

[22] P. T. TIN, et al. Throughput enhancement for multi-hop decode-and-forward protocol using interference cancellation with hardware imperfection. *Alexandria Engineering Journal*, vol. 61, no. 8, pp. 5837-5849, 2022. DOI: 10.1016/j.aej.2021.11.008.

[23] T. N. NGUYEN, et al. Physical Layer Security in AF-Based Cooperative SWIPT Sensor Networks. *IEEE Sensors Journal*, vol. 23, no. 1, pp. 689 - 705, 2023. DOI: 10.1109/JSEN.2022.3224128.

[24] YANG, L., YANG, Y., HASNA, M. O. and ALOUINI, M.-S. Coverage, probability of SNR gain, and DOR analysis of RIS-aided communication systems. *IEEE Wireless Communications Letters*, vol. 9, iss. 8, pp. 1268-1272, 2020. DOI: 10.1109/LWC.2020.2987798.

[25] BASAR, E., RENZO, M.-D., ROSNY, J.-D., DEBBAH, M., ALOUINI, M.-S. and ZHANG, R. Wireless communications through reconfigurable intelligent surfaces. *IEEE Access*, vol. 7, pp. 116753-116773, 2019. DOI: 10.1109/ACCESS.2019.2935192.

[26] YUE, X. and LIU, Y. Performance analysis of intelligent reflecting surface assisted NOMA networks. *IEEE Transactions on Wireless Communications*, vol. 21, no. 4, pp. 2623-2636, 2021. DOI: 10.1109/TWC.2021.3114221.

[27] SANG, N.Q., T.N. NGUYEN, and L.T. TU. On the Security and Reliability Performance of SWIPT-enabled Full-Duplex Relaying in the Non-Orthogonal Multiple Access Networks.

Journal of Information and Telecommunication, vol. 7, no. 4, pp. 462-476, 2023. DOI: 10.1080/24751839.2023.2218046.

[28] NGUYEN, H.N., DANG, H.P., LE, S.P., LE, T.D., DO, D.T., VOZNAK, M. and ZDRALEK, J. Enabling D2D transmission mode with energy harvesting and information transfer in heterogeneous networks. *Advances in Electrical and Electronic Engineering*, vol. 16, no. 2, pp.178-184, 2018. DOI: 10.15598/aeee.v16i2.2393.

[29] HUYNH, V. V., TAN-LOC, N., QUOC-PHU, M., SEVCIK, L., NGUYEN, H. S., and VOZNAK, M. Energy efficiency maximization of two-time-slot and three-time-slot two-way relay-assisted device-to-device underlaying cellular networks. *Energies*, vol. 13, no. 13, art.no. 3422, 2020. DOI: 10.3390/en13133422.

[30] A-T. LE, T.N. NGUYEN, L-T. TU, T-P. TRAN, T.T. DUY, M.VOZNAK, and Z.DING. Performance Analysis of RIS-Assisted Ambient Backscatter Communication Systems. *IEEE Wireless Communications Letters*, vol. 13, no.3, pp.791-795, 2023. DOI: 10.1109/LWC.2023.3344113.

[31] S. LI, L. BARIAH, S. MUHAIDAT, A. WANG AND J. LIANG. Outage Analysis of NOMA-Enabled Backscatter Communications With Intelligent Reflecting Surfaces. *IEEE Internet of Things Journal*, vol. 9, no. 16, pp. 15390-15400, 2022. DOI: 10.1109/JIOT.2022.3150418.

[32] PEPPAS K.-P. A new formula for the average bit error probability of dual-hop amplify-and-forward relaying systems over generalized shadowed fading channels. *IEEE Wireless Communications Letters*, vol. 1, no. 2, pp. 85-88. ISSN 2162-2337, 2012. DOI: 10.1109/WCL.2012.012712.110092.

[33] MATHAI, A.M., SAXENA, R.K. and HAUBOLD, H.J. *The H-function: theory and applications.* New York, NY, USA: Springer, 2009. DOI: 10.1007/978-1-4419-0916-9.

[34] LEI, H., ANSARI, I.S., PAN, G., ALOMAIR, B. and ALOUINI, M.-S. Secrecy Capacity Analysis Over $\alpha - \mu$ Fading Channels. *IEEE Communications Letters.* 2017, vol. 21, iss. 6, pp. 1445-1448. ISSN 1089-7798. DOI: 10.1109/LCOMM.2017.2669976.

[35] LI, X., ZHENG, Y., ZENG, M., LIU, Y. and DOBRE, O.-A. Enhancing Secrecy Performance for STAR-RIS NOMA Networks. *IEEE Transactions on Vehicular Technology*, vol. 72, iss. 2, pp. 2684-2688, 2022. DOI: 10.1109/TVT.2022.3213334.

[36] LIU, H., LI, G., LI, X., LIU, Y., HUANG, G. and DING, Z. Effective Capacity Analysis of STAR-RIS-Assisted NOMA Networks. *IEEE Wireless Communications Letters*, vol. 11, no. 9, pp. 1930-1934, 2022. DOI: 10.1109/LWC.2022.3188443.

[37] V. D. PHAN, et al.Performance of Cooperative Communication System With Multiple Reconfigurable Intelligent Surfaces Over Nakagami-m Fading Channels. *IEEE Access*, vol. 10, pp. 9806-9816, 2022. DOI: 10.1109/ACCESS.2022.3144364.

[38] B. C. NGUYEN, et al. Cooperative Communications for Improving the Performance of Bidirectional Full-Duplex System With Multiple Reconfigurable Intelligent Surfaces. *IEEE Access*, vol. 9, pp. 134733-134742, 2021. DOI: 10.1109/ACCESS.2021.3114713.

[39] PRUDNIKOV, A., BRYCHKOV, Y., BRYCHKOV, I. and MARICHEV, O. *Integrals and Series. Volume 3: More Special Functions*, ser. Integrals and Series. Gordon and Breach Science Publishers, 1986.

[40] GRADSHTEYN, I. S. and RYZHIK, I. M. *Table of Integrals, Series and Products*, 6th ed. New York, NY, USA: Academic Press, 2000.

[41] MITTAL, P. and GUPTA, K. An integral involving generalized function of two variables. *Proceedings of the Indian academy of sciences-section A.* 1972, vol. 75, no. 3, pp. 117-123. ISSN 0973-7685. DOI: 10.1007/BF03049732.

[42] T. N. NGUYEN, et al. Outage Performance of Satellite Terrestrial Full-Duplex Relaying Networks With co-Channel Interference.*IEEE Wireless Communications Letters*, vol. 11, no. 7, pp. 1478-1482, 2022. DOI: 10.1109/LWC.2022.3175734.

[43] Q-S. NGUYEN, U-V.L. ANH, T.N. NGUYEN, T-T. NGUYEN, AND M. VOZNAK. Short Packet Communications for Relay Systems with Co-channel Interference at Relay: Performance Analysis and Power Control. *IEEE Access*, vol. 12, pp. 63452-63461, 2024. DOI: 10.1109/ACCESS.2024.3396642.

[44] A-T. LE, et.al. Physical layer security analysis for RIS-aided NOMA systems with non-colluding eavesdroppers. *Computer Communications*, vol. 219, pp. 194-203, 2024. DOI: 10.1016/j.comcom.2024.03.011.

[45] T.N. NGUYEN, et al. Multisource Power Splitting Energy Harvesting Relaying Network in Half-Duplex System over Block Rayleigh Fading Channel: System Performance Analysis. *Electronics*, vol. 8, no. 1, art.no.67, 2019. DOI: 10.3390/electronics8010067.